Pergamon

0045-7930(94)00032-8

Computers Fluids Vol. 24, No. 3, pp. 227–238, 1995

0045-7930/95 $9.50 + 0.00

A NEW k–ϵ EDDY VISCOSITY MODEL FOR HIGH REYNOLDS NUMBER TURBULENT FLOWS

TSAN-HSING SHIH, WILLIAM W. LIOU, AAMIR SHABBIR, ZHIGANG YANG and JIANG ZHU

Center for Modeling of Turbulence and Transition, Institute for Computational Mechanics in Propulsion, NASA Lewis Research Center, Cleveland, OH 44135, U.S.A.

(Received 31 January 1994; in revised form 28 September 1994)

Abstract—A new k–ϵ eddy viscosity model, which consists of a new model dissipation rate equation and a new realizable eddy viscosity formulation, is proposed in this paper. The new model dissipation rate equation is based on the dynamic equation of the mean-square vorticity fluctuation at large turbulent Reynolds number. The new eddy viscosity formulation is based on the realizability constraints; the positivity of normal Reynolds stresses and the Schwarz' inequality for turbulent shear stresses. We find that the present model with a set of unified model coefficients can perform well for a variety of flows. The flows that are examined include: (i) rotating homogeneous shear flows; (ii) boundary-free shear flows including a mixing layer, planar and round jets; (iii) a channel flow, and flat plate boundary layers with and without a pressure gradient; and (iv) backward facing step separated flows. The model predictions are compared with available experimental data. The results from the standard k–ϵ eddy viscosity model are also included for comparison. It is shown that the present model is a significant improvement over the standard k–ϵ eddy viscosity model.

1. INTRODUCTION

The main task in developing a k–ϵ eddy viscosity model is to provide an appropriate eddy viscosity formulation and a model dissipation rate equation. The standard k–ϵ eddy viscosity model, which is widely used in computational fluid dynamics, performs quite well for boundary layer flows but not for flows with a high mean shear rate or a massive separation, because in these cases the eddy viscosity is overpredicted by the standard eddy viscosity formulation. In addition, the standard model dissipation rate equation does not always give the appropriate length scale for turbulence. For example, the well-known anomaly about the spreading rate of a planar jet versus a round jet is mainly due to the model dissipation rate equation. In order to improve the ability of the k–ϵ eddy viscosity model to predict complex turbulent flows, these deficiencies in the existing k–ϵ eddy viscosity model should be removed. The purpose of this study is to propose new formulations for both the model dissipation rate equation and the eddy viscosity that can significantly improve the performance of the k–ϵ eddy viscosity model.

The exact dissipation rate equation can be written as,

$$\epsilon_{,t} + U_i\epsilon_{,i} = \nu\epsilon_{,ii} - (\overline{\epsilon' u_i})_{,i} - \frac{2\nu}{\rho}(\overline{p_{,k}u_{i,k}})_{,i} - 2\nu\overline{u_j u_{i,k}}U_{i,kj} - 2\nu\overline{u_{i,k}u_{j,k}}U_{i,j} - 2\nu\overline{u_{i,j}u_{i,k}}U_{j,k} - 2\nu\overline{u_{i,k}u_{j,k}u_{i,j}} - 2\nu^2\overline{u_{i,jk}u_{i,jk}} \quad (1a)$$

where $\epsilon = \nu\overline{u_{i,j}u_{i,j}}$, $\epsilon' = \nu u_{i,j}u_{i,j}$ and $(\,)_{,t}$, $(\,)_{,i}$ stand for the derivatives with respect to t and x_i. All the terms on the right hand side of equation (1a), except the viscous diffusion term $\nu\epsilon_{,ii}$, are new unknowns. Thus, they must be modeled before this equation can be used for applications. Modeling of these new unknowns, which are related to the small scales of turbulence, is extremely difficult. Therefore, in the literature, equation (1a) is usually not considered as a useful equation to work with. Instead, one creates a simple model dissipation rate equation which has a structure similar to that of the turbulent kinetic energy equation. That is, the dissipation rate equation also has generation and destruction terms which are assumed to be proportional to the production and

dissipation of turbulent kinetic energy divided by the large eddy turn-over time, k/ϵ. With this assumption, the resulting model dissipation rate equation can be written in the following form:

$$\epsilon_{,t} + U_i\epsilon_{,i} = \nu\epsilon_{,ii} - (\overline{\epsilon' u_i})_{,i} - C_{\epsilon 1}\frac{\epsilon}{k}\overline{u_i u_j}U_{i,j} - C_{\epsilon 2}\frac{\epsilon^2}{k} \tag{1b}$$

Equation (1b) is the standard form of the model dissipation rate equation which has been widely used in various turbulence closure schemes. In addition, several modified versions of equation (1b) have also been proposed for different applications, for example, in near-wall turbulent flows [1–4] and in rotating turbulent flows [5]. Recently, Lumley [6] proposed a dissipation rate equation based on the concept of non-equilibrium spectral energy transfer due to the interactions between eddies of different sizes. A new transport equation for an inverse time scale has also been suggested in conjunction with his new ϵ equation which is of a different form from that of equation (1b). This model mimics the physics of the statistical energy transfer from large eddies to small eddies and was successful in the prediction of some turbulent free shear flows [6]. In the present study, we explore the possibility of deriving a new model form for the dissipation rate equation which is not only physically more related to the original ϵ equation but also simpler and more robust than the standard dissipation equation (1b). This is achieved by first developing a model equation for the dynamic equation of the mean-square vorticity fluctuation $\overline{\omega_i\omega_i}$. Once the dynamic equation for $\overline{\omega_i\omega_i}$ is modeled, a model dissipation rate equation can be readily obtained by using the relation $\epsilon = \nu\overline{\omega_i\omega_i}$ at large Reynolds number.

The standard eddy viscosity formulation for incompressible turbulence is

$$-\overline{u_i u_j} = -\tfrac{2}{3}k\delta_{ij} + \nu_T(U_{i,j} + U_{j,i}) \tag{2a}$$

$$\nu_T = C_\mu\frac{k^2}{\epsilon} \tag{2b}$$

$$C_\mu = 0.09 \tag{2c}$$

It has been known for long that this model will become non-realizable in the case of large mean strain rate (e.g., $Sk/\epsilon > 3.7$ where $S = \sqrt{2S_{ij}S_{ij}}$), because the normal stresses can become negative and the Schwarz' inequality for shear stresses can be violated. To insure realizability, the model coefficient C_μ must not be a constant and must be related to the mean strain rate. In fact, the experiments on boundary layer and homogeneous shear flows also show that the value of C_μ is quite different in each case. For example, C_μ is about 0.09 in the inertial sublayer of a flat boundary layer is which $Sk/\epsilon = 3.3$, and C_μ is about 0.5 in a homogeneous shear flow of $Sk/\epsilon = 6$. According to the above considerations, a new formulation for C_μ, which was suggested by Reynolds [7] and Shih *et al.* [8], is adopted in this paper.

In the following sections, we will first describe the development of a new model dissipation rate equation, and then the development of the new eddy viscosity formulation. The performance of the new model will be examined in a variety of flows which include rotating homogeneous shear flows, boundary-free shear flows (e.g., a mixing layer, planar and round jets), a channel flow, boundary layers with and without pressure gradients, and backward facing step separated flows.

2. DEVELOPMENT OF THE NEW DISSIPATION RATE EQUATION

2.1. *Dynamic equation for* $\overline{\omega_i\omega_i}$

The exact equation for $\overline{\omega_i\omega_i}$ is

$$\left(\frac{\overline{\omega_i\omega_i}}{2}\right)_{,t} + U_j\left(\frac{\overline{\omega_i\omega_i}}{2}\right)_{,j} = \nu\left(\frac{\overline{\omega_i\omega_i}}{2}\right)_{,jj} - \tfrac{1}{2}(\overline{u_j\omega_i\omega_i})_{,j}$$
$$+ \overline{\omega_i u_{i,j}}\Omega_j - \overline{u_j\omega_i}\Omega_{i,j} + \overline{\omega_i\omega_j}U_{i,j}$$
$$+ \overline{\omega_i\omega_j u_{i,j}} - \nu\overline{\omega_{i,j}\omega_{i,j}} \tag{3}$$

where u_i and U_i are the fluctuating and mean velocities, and ω_i and Ω_i are the fluctuating and mean vorticities which are defined by

$$\omega_i = \epsilon_{ijk} u_{k,j}, \quad \Omega_i = \epsilon_{ijk} U_{k,j} \tag{4}$$

and

$$S_{ij} = \tfrac{1}{2}(U_{i,j} + U_{j,i}), \quad \Omega_{ij} = \tfrac{1}{2}(U_{i,j} - U_{j,i})$$

Tennekes and Lumley [9] clearly described the physical meaning of each term in equation (3). The first two terms on the right hand side represent the viscous transport and the turbulent transport of $\overline{\omega_i \omega_i}$, respectively. The third term is the source term which is produced by fluctuating vortex stretching and mean vorticity. This term also appears in the equation for $\Omega_i \Omega_i$ with the same sign, hence, it will either increase or decrease $\Omega_i \Omega_i$ and $\overline{\omega_i \omega_i}$ simultaneously. The fourth term represents the vorticity exchange between $\overline{\omega_i \omega_i}$ and $\Omega_i \Omega_i$, because it appears with opposite sign in the equation for $\Omega_i \Omega_i$. The fifth term represents the source produced by mean vortex stretching. The sixth and seventh terms are the production due to fluctuating vortex stretching and the dissipation due to the viscosity of the fluid, respectively. Tennekes and Lumley have shown that, at sufficiently high turbulent Reynolds numbers, the sixth and the seventh terms in equation (3) are the largest terms and are of order:

$$\overline{\omega_i \omega_j u_{i,j}}, \nu \overline{\omega_{i,j} \omega_{i,j}} \approx \mathcal{O}\left(\frac{u^3}{l^3} R_t^{3/2} \right)$$

All the remaining terms on the right hand side, except the second term, are smaller, either of order (u^3/l^3) or $(u/l)^3 R_t^{1/2}$. In the above analysis, "$\mathcal{O}$" denotes the order of magnitude, $R_t = ul/\nu$ is the turbulent Reynolds number, and u and l are the characteristic velocity and length scales of turbulence, respectively. If the terms of order $(u^3/l^3)R_t$ or larger were kept in equation (3), then the evolution of $\overline{\omega_i \omega_i}$ would be described by the following equation,

$$\left(\frac{\overline{\omega_i \omega_i}}{2} \right)_{,t} + U_j \left(\frac{\overline{\omega_i \omega_i}}{2} \right)_{,j} = -\tfrac{1}{2}(\overline{u_j \omega_i \omega_i})_{,j} + \overline{\omega_i \omega_j u_{i,j}} - \nu \overline{\omega_{i,j} \omega_{i,j}} \tag{5}$$

As pointed out by Tennekes and Lumley, at very large Reynolds numbers, equation (5) becomes,

$$\overline{\omega_i \omega_j u_{i,j}} = \nu \overline{\omega_{i,j} \omega_{i,j}} \tag{6}$$

Or equivalently, production equals dissipation. This relation indicates that the term $\overline{\omega_i \omega_j u_{i,j}}$ is always positive. In addition, it indicates that there is a new length scale created by the vortex stretching which is related to the derivative of fluctuating vorticity. The vortex stretching tends to reduce the size of eddies and to create a broad spectrum of eddy sizes. However, this process must end at a certain level of eddy size because of the smoothing effect of viscosity. We expect that the terminal eddy size is the Kolmogorov microscale which corresponds to the length scale for the derivative of fluctuating vorticity $\omega_{i,j}$. This can be easily verified from equation (6).

2.2. *Modeling of the dynamic equation for* $\overline{\omega_i \omega_i}$

2.2.1. Modeling of $\overline{\omega_i \omega_j u_{i,j}}$. We first define a fluctuating anisotropic tensor b_{ij}^{ω} using $\omega_i \omega_j$

$$b_{ij}^{\omega} = \frac{\omega_i \omega_j}{\omega_k \omega_k} - \tfrac{1}{3} \delta_{ij} \tag{7}$$

then

$$\overline{\omega_i \omega_j u_{i,j}} = \overline{b_{ij}^{\omega} \omega_k \omega_k u_{i,j}} \tag{8}$$

where the continuity equation, $u_{i,i} = 0$, has been used. We expect that the vortex stretching tends to align vortex lines with the strain rate and that the anisotropy b_{ij}^{ω} is mainly due to the anisotropy

of the fluctuating strain rate; hence, the anisotropy b_{ij}^{ω} may be assumed to be proportional to the strain rate s_{ij}. That is,

$$b_{ij}^{\omega} \propto \frac{s_{ij}}{s}, \tag{9}$$

where

$$s = (2s_{ij}s_{ij})^{1/2}, \quad s_{ij} = (u_{i,j} + u_{j,i})/2$$

This leads to

$$\overline{\omega_i\omega_j u_{i,j}} \propto \overline{\omega_k\omega_k \frac{s_{ij}u_{i,j}}{s}} \propto \overline{\omega_k\omega_k s} \tag{10}$$

If we further assume that $\omega_k\omega_k$ and $(2s_{ij}s_{ij})^{1/2}$ are well correlated, we may write

$$\overline{\omega_i\omega_j u_{i,j}} \propto \overline{\omega_k\omega_k}\sqrt{\overline{2s_{ij}s_{ij}}} \tag{11}$$

Noting that $\overline{\omega_i\omega_i} = 2\overline{s_{ij}s_{ij}}$ at large Reynolds numbers, we may also write

$$\overline{\omega_i\omega_j u_{i,j}} \propto \overline{\omega_k\omega_k}\sqrt{\overline{\omega_i\omega_i}} = \frac{\omega_k\omega_k\overline{\omega_i\omega_i}}{\sqrt{\overline{\omega_i\omega_i}}} \tag{12}$$

Equations (11) and (12) both indicate that the model for $\overline{\omega_i\omega_j u_{i,j}}$ is of order $(u^3/l^3)R_t^{3/2}$ as it should be.

2.2.2. Modeling of $\overline{\omega_i\omega_j u_{i,j}} - \nu\overline{\omega_{i,j}\omega_{i,j}}$. Equation (5) indicates that $\overline{\omega_i\omega_j u_{i,j}} - \nu\overline{\omega_{i,j}\omega_{i,j}}$ must be of order $(u^3/l^3)R_t$, because that is the order of the magnitude for the other terms in equation (5). Therefore, the model of $-\nu\overline{\omega_{i,j}\omega_{i,j}}$ must cancel $\overline{\omega_k\omega_k}\sqrt{\overline{2s_{ij}s_{ij}}}$ (or $\overline{\omega_j\omega_k}\,\overline{\omega_i\omega_i}/\sqrt{\overline{\omega_i\omega_i}}$) in such a way that their difference is smaller than $\overline{\omega_k\omega_k}\sqrt{\overline{2s_{ij}s_{ij}}}$ (or $\overline{\omega_k\omega_k}\,\overline{\omega_i\omega_i}/\sqrt{\overline{\omega_i\omega_i}}$) by an order of $R_t^{1/2}$. This suggests that the sum of these two terms can be related to the following two terms:

$$\overline{\omega_k\omega_k}S, \quad \frac{\overline{\omega_k\omega_k}\,\overline{\omega_i\omega_i}}{\frac{k}{\nu} + \sqrt{\overline{\omega_i\omega_i}}} \tag{13}$$

since both the ratio of s to S and the ratio of k/ν to $\sqrt{\omega_i\omega_i}$ are of order $R_t^{1/2}$. Here, $k\,(\approx u^2)$ denotes the turbulent kinetic energy and S is the mean strain rate $(\sqrt{2S_{ij}S_{ij}})$. As a result, the dynamic equation for fluctuating vorticity can be modeled as

$$\left(\frac{\overline{\omega_i\omega_i}}{2}\right)_{,t} + U_j\left(\frac{\overline{\omega_i\omega_i}}{2}\right)_{,j} = -\tfrac{1}{2}(\overline{u_j\omega_i\omega_i})_{,j} + C_1\overline{\omega_k\omega_k}S - C_2\frac{\overline{\omega_k\omega_k}\,\overline{\omega_i\omega_i}}{\frac{k}{\nu} + \sqrt{\overline{\omega_i\omega_i}}} \tag{14}$$

Note that the denominator of the last term in equation (14) should be k/ν for large Reynolds number turbulence since the term $\sqrt{\overline{\omega_i\omega_i}}$ is negligible compared to k/ν. However, we keep it there in case k vanishes somewhere in the flow field to prevent unnecessary singularity. This also reflects the fact that the parent term of the model, equation (12), shows no singularity anywhere in the flow field. It should also be pointed out that the sum of last two terms in equation (14) models the last two terms in equation (5) as a whole and should not be viewed as a model for either individual term.

2.3. Modeling of the dissipation rate equation

Noting that at large Reynolds number $\epsilon = \nu\overline{\omega_i\omega_i}$ and multiplying equation (14) by ν, we readily obtain a modeled dissipation rate equation,

$$\epsilon_{,t} + U_j\epsilon_{,j} = -(\overline{u_j\epsilon'})_{,j} + C_1S\epsilon - C_2\frac{\epsilon^2}{k + \sqrt{\nu\epsilon}} \tag{15}$$

Table 1. Anisotropy component b_{12}

	Exp.	Standard	Present
Boundary layer b_{12}	−0.149	−0.149	−0.149
Homoge. shear b_{12}	−0.142	−0.274	−0.18

The model coefficients, C_1 and C_2, are expected to be independent of the Reynolds number as the Reynolds number becomes large. We note that C_1 and C_2 may be affected by solid body rotation imposed on turbulence through the reduction of fluctuation vortex stretching, $\overline{\omega_i \omega_j u_{i,j}}$, as was shown by Bardina [5]; however, this effect is rather weak compared to the other mechanisms. For example, Reynolds stresses will first be substantially affected by rotation and result in a substantial change of the turbulent field, say k, as shown in the calculation of the rotating homogeneous shear flows in Section 4.1. This will also affect the evolution of ϵ through, say, k. The signs of C_1 and C_2 can be easily determined. For example, in a decaying grid turbulence, only the last term on the right hand side of equation (15) is non-zero and must be negative, hence C_2 must be positive. For the case of homogeneous shear flow, both the turbulent kinetic energy and its dissipation rate increase with time so that the "source" term in equation (15) must be positive, hence C_1 must be positive. In fact, these two types of flows [10, 11] will be used for determining the coefficients C_1 and C_2.

The difference between the present model dissipation rate equation, equation (15), and the standard model dissipation rate equation, equation (1b), is the "source" term. The Reynolds stresses do not appear in equation (15). Consequently, the present model dissipation rate equation will be more robust than the standard model dissipation rate equation when it is used in conjunction with second-order closure schemes, since S normally behaves better than the Reynolds stresses in numerical calculations, especially for the cases with poor initial conditions. In addition, the present form of the "production" term is similar to that proposed by Lumley [6] which is based on the concept of spectral energy transfer. We believe that the present form of the model dissipation rate equation describes the turbulent vortex stretching and dissipation terms more appropriately.

Equation (15) can be applied in conjunction with any level of turbulence closure; however, the turbulent transport term $(\epsilon' u_i)_{,i}$ needs to be modeled differently at different levels of turbulence closure. Here, we apply equation (15) to a realizable eddy viscosity model which will be described in the next section, and where $(\overline{\epsilon' u_i})_{,i}$ is modeled as

$$(\overline{\epsilon' u_i})_{,i} = -\left(\frac{\nu_T}{\sigma_\epsilon}\epsilon_{,i}\right)_{,i} \tag{16}$$

The model coefficients C_1, C_2 and σ_ϵ will be determined later.

3. REALIZABLE EDDY VISCOSITY MODEL

Shih *et al.* [8] proposed a realizable Reynolds stress algebraic equation model. Its linear form represents an isotropic eddy viscosity model:

$$-\overline{u_i u_j} = \nu_T(U_{i,j} + U_{j,i}) - \tfrac{2}{3}k\delta_{ij} \tag{17.1}$$

$$\nu_T = C_\mu \frac{k^2}{\epsilon} \tag{17.2}$$

Here the coefficient C_μ is not a constant. The experimental as well as DNS data on the inertial sublayer of a channel or boundary layer flow suggest that $C_\mu = 0.09$. On the other hand, for a

Table 2. Model coefficients

σ_k	σ_ϵ	C_1	C_2	C_μ	A_0
1.0	1.2	equation (25)	1.9	equation (19)	4.0

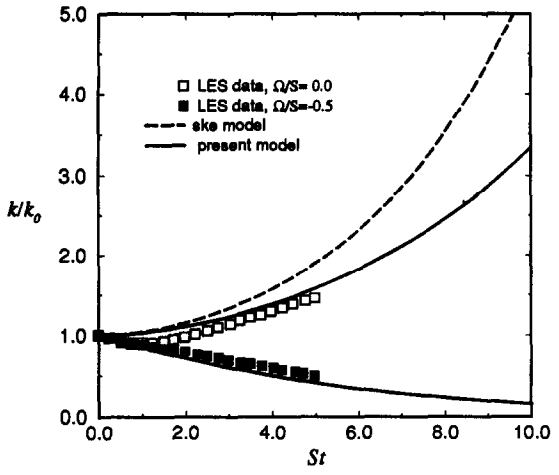

Fig. 1. Time evolution of turbulent kinetic energy in rotating homogeneous shear flows. $\Omega/S = 0.0$ and -0.5.

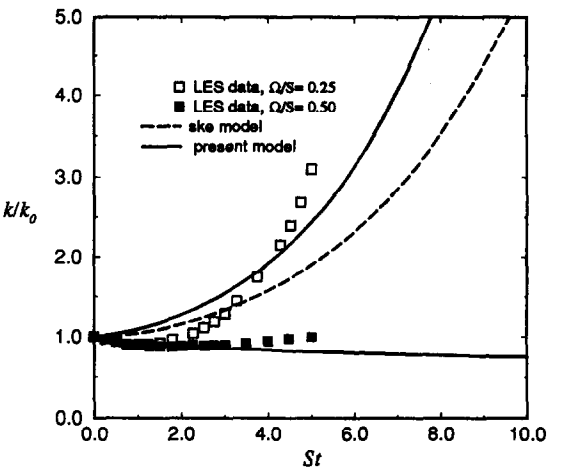

Fig. 2. Time evolution of turbulent kinetic energy in rotating homogeneous shear flows. $\Omega/S = 0.25$ and 0.5.

homogeneous shear flow, $C_\mu = [-(\overline{uv})/k]/(k/\epsilon)(\partial U/\partial y)$ which is about 0.05 from the experiment of Tavoularis and Corrsin [11]. Based on the realizability conditions:

$$\overline{u_\alpha^2} \geqslant 0 \quad (\alpha = 1, 2, 3)$$

$$\frac{\overline{u_\alpha u_\beta^2}}{\overline{u_\alpha^2}\,\overline{u_\beta^2}} \leqslant 1 \quad (\alpha = 1, 2, 3;\ \beta = 1, 2, 3) \tag{18}$$

Reynolds [7] and Shih *et al.* [8] proposed the following formulation for the coefficient of C_μ:

$$C_\mu = \frac{1}{A_0 + A_s U^{(*)} \dfrac{k}{\epsilon}} \tag{19}$$

In the formulation of Shih *et al.* [8],

$$U^{(*)} = \sqrt{S_{ij} S_{ij} + \tilde{\Omega}_{ij} \tilde{\Omega}_{ij}}$$

$$\tilde{\Omega}_{ij} = \Omega_{ij} - 2\epsilon_{ijk}\omega_k \tag{20}$$

$$\Omega_{ij} = \bar{\Omega}_{ij} - \epsilon_{ijk}\omega_k$$

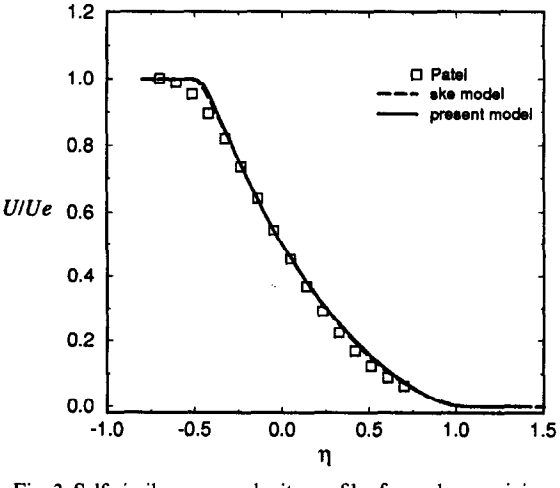

Fig. 3. Self-similar mean velocity profiles for a planar mixing layer.

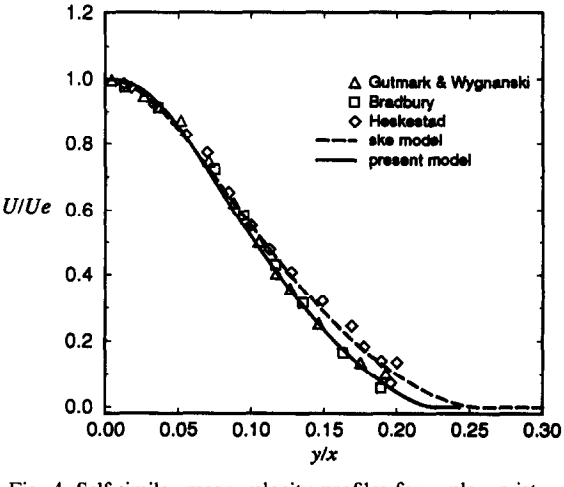

Fig. 4. Self-similar mean velocity profiles for a planar jet.

where $\overline{\Omega_{ij}}$ is the mean rotation rate viewed in a rotating reference frame with the angular velocity ω_k. The parameter A_s is determined by

$$A_s = \sqrt{6}\cos\phi, \quad \phi = \tfrac{1}{3}\arccos(\sqrt{6}W)$$

$$W = \frac{S_{ij}S_{jk}S_{ki}}{\tilde{S}^3} \quad \tilde{S} = \sqrt{S_{ij}S_{ij}} \tag{21}$$

3.1. Calibration of the model coefficient A_0

The new eddy viscosity formulation of equations (17), (19), (20) and (21) satisfies the realizability constraints equation (18), and hence is a realizable model. The only undetermined coefficient is A_0. If we assume for simplicity that A_0 is a constant, then the value of A_0 can be calibrated by one of the simple flows, such as a homogeneous shear flow or a boundary layer flow. The value of A_0 will depend on the flow used for the calibration. Here, we choose a boundary layer flow in hope that the model will be able to reproduce the log-law of the inertial sublayer. This leads to $A_0 = 4.0$ which corresponds to $C_\mu = 0.09$ in the inertial sublayer. For the homogeneous shear flow of Tavoularis and Corrsin [11], equation (19) gives $C_\mu = 0.06$ which is much closer to the experimental value of 0.05 than that of the standard $C_\mu = 0.09$. The component of the anisotropy b_{12} $(\overline{uv}/2k)$ for both the flows is listed in Table 1 which shows that the present form of C_μ also produces reasonable b_{12} compared to the standard form of C_μ.

Now let us go back to the modeled k and ϵ equations,

$$k_{,t} + U_j k_{,j} = \left(\frac{\nu_T}{\sigma_k} k_{,j}\right)_{,j} - \overline{u_i u_j} U_{i,j} - \epsilon \tag{22}$$

$$\epsilon_{,t} + U_j \epsilon_{,j} = \left(\frac{\nu_T}{\sigma_\epsilon} \epsilon_{,j}\right)_{,j} + C_1 S\epsilon - C_2 \frac{\epsilon^2}{k + \sqrt{\nu\epsilon}} \tag{23}$$

and determine the coefficients in equation (23).

3.2. Calibration of the model coefficients C_1, C_2 and σ_ϵ

In decaying grid turbulence at large Reynolds number, the equations for turbulent kinetic energy k and its dissipation rate ϵ are

$$k_{,t} = -\epsilon, \quad \epsilon_{,t} = -C_2 \frac{\epsilon^2}{k}$$

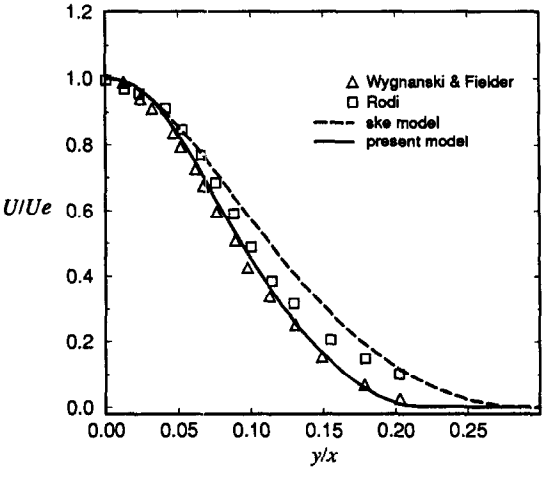

Fig. 5. Self-similar mean velocity profiles for a round jet.

Table 3. The spreading rates of turbulent free shear flows

Case	Measurements	ske	Present
Mixing layer	0.13–0.17	0.152	0.151
Planar jet	0.105–0.11	0.109	0.105
Round jet	0.085–0.095	0.116	0.094

Let

$$\frac{k}{k_0}=\left(\frac{t}{t_0}\right)^{-n}, \quad \frac{\epsilon}{\epsilon_0}=\left(\frac{t}{t_0}\right)^{-\alpha}$$

the following equations can be obtained from the k and ϵ equations:

$$\alpha = n+1, \quad C_2=\frac{n+1}{n} \tag{24}$$

Experiments [10] show that the decay exponent n varies from 1.08 to 1.30. In this study we choose $C_2 = 1.9$ which corresponds to $n = 1.11$. After C_2 is chosen, we use the experimental data of homogeneous shear flow [11] and boundary layer flow to determine the coefficient C_1 which is found to be a simple function of the time scale ratio of the turbulence to the mean strain, η:

$$C_1 = \max\left\{0.43, \frac{\eta}{5+\eta}\right\} \tag{25}$$

where

$$\eta = \frac{Sk}{\epsilon}, \quad S=\sqrt{2S_{ij}S_{ij}}$$

The value of σ_ϵ will be estimated using the log-law in a boundary layer flow. The following relations hold in the inertial sublayer:

$$\frac{U}{u_\tau}=\frac{1}{k}\log\frac{u_\tau y}{\nu}+C$$

$$-\overline{uv}\approx u_\tau^2, \quad -\overline{uv}\frac{\partial U}{\partial y}\approx\epsilon \tag{26}$$

Analyzing the dissipation rate equation in the log-law region, we obtain

$$\sigma_\epsilon=\frac{k^2}{C_2\sqrt{C_\mu}-C_1}=1.20 \tag{28}$$

where the von Karman constant $k = 0.41$. The model coefficients are summarized in Table 2.

4. MODEL APPLICATIONS

The results of turbulent flow calculations using the proposed new turbulence model are shown in this section. These include (i) rotating homogeneous shear flows, (ii) boundary-free shear

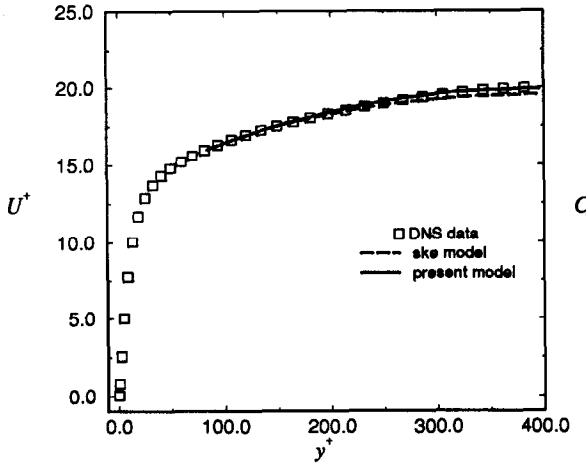

Fig. 6. Mean velocity profile for turbulent channel flow at $Re_\tau = 395$.

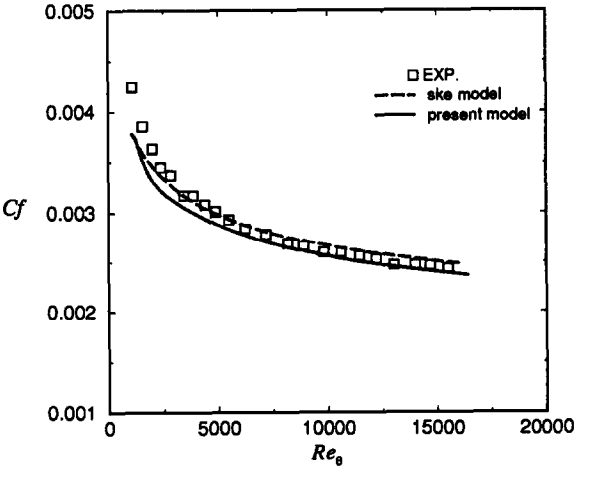

Fig. 7. Skin friction coefficient for the zero pressure gradient turbulent boundary layer.

flows, (iii) a channel flow and boundary layers with and without pressure gradients, and (iv) backward-facing step flows. The results of the present and the standard k–ϵ models are compared with DNS, LES and experiments.

4.1. *Rotating homogeneous shear flows*

The comparisons are made with the large eddy simulation of Bardina *et al.* [5] for four different cases of Ω/S (which are $\Omega/S = 0.0$, $\Omega/S = -0.50, \Omega/S = 0.25$, and $\Omega/S = 0.50$). The initial conditions in all these cases correspond to isotropic turbulence and $\epsilon_0/Sk_0 = 0.296$. Figure 1 compares the evolution of turbulence kinetic energy, normalized by its initial value k_0, with the non-dimensional time St for the cases of $\Omega/S = 0.0$ and $\Omega/S = -0.5$. For the first case both the present and the standard k–ϵ (denoted by ske hereafter) models show the trends exhibited by LES, with the present model closer to the LES data. For the second case the ske model does not show the effect of rotation on turbulence as it gives the same growth rate of turbulence kinetic energy as it did for the no rotation case, a result which is already known. On the other hand the present model is in reasonable agreement with the LES data as it shows the decay of the turbulence kinetic energy with time. Figure 2 compares the evolution of turbulence kinetic energy for $\Omega/S = 0.25$ and $\Omega/S = 0.5$. For the first of these cases the LES shows that the growth rate of the turbulence kinetic energy is increased over the no rotation rate case. The present model is able to pick up this trend while the ske model does not. For the case of $\Omega/S = 0.5$ the agreement between the present model and the LES is not as good but the present model still performs a lot better than the ske model.

4.2. *Boundary-free shear flows*

Calculations using the present and the ske models were performed for a mixing layer, a planar and a round jet. Grid-independence studies (with 100 and 150 grid points across the shear layer) show that the self-similar profiles are essentially the same. Figures 3, 4 and 5 show the comparisons of the self-similar mean velocity profiles from the model predictions, obtained by using the fine grid, and the various measurements for the mixing layer, planar and round jets, respectively. The comparisons of the Reynolds shear stress and turbulent kinetic energy profiles can be found in Shih *et al.* [12] and are not included here due to space limitation. For the mixing layer, the results are shown in a self-similar coordinate η defined as

$$\eta = \frac{y - y_{0.5}}{y_{0.9} - y_{0.1}}$$

where $y_{0.1}$, $y_{0.5}$, and $y_{0.9}$ denote the locations where the ratio of the local mean velocity to that of the free stream are 0.1, 0.5, and 0.9, respectively. Figure 3 shows that the mean velocity profiles

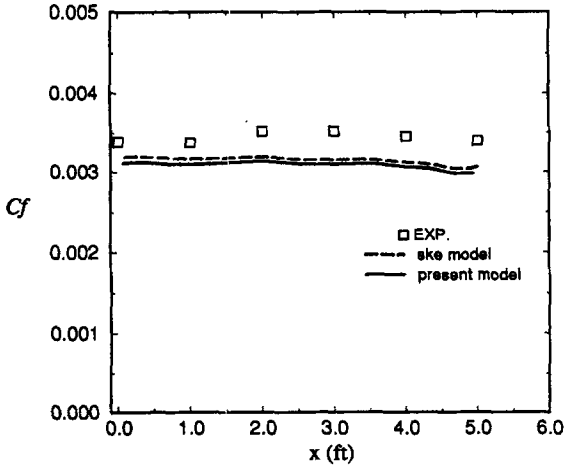

Fig. 8. Skin friction coefficient for the Herring and Norbury flow [20].

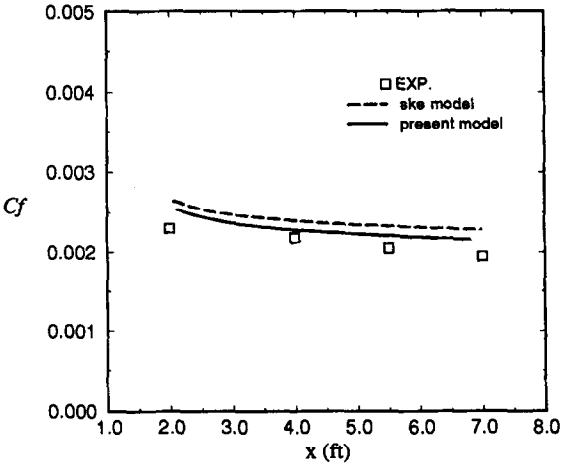

Fig. 9. Skin friction coefficient for the Bradshaw flow [21].

of the mixing layer predicted by either the present model or the ske model agree well with experimental data of Patel [13]. The present model, however, gives better predictions of the turbulent kinetic energy and the Reynolds shear stress distributions than the ske model. This is especially true for their peak levels. The predictions for the planar jet are shown in Fig. 4. The model predictions are compared with the measurements of Gutmark and Wygnanski [14], Bradbury [15], and Hekestad [16]. The predictions given by both the present model and the ske model agree well with the experimental data. For the round jet, the comparisons are made between the model predictions and the measurements of Wygnanski and Fielder [17] and Rodi [18] and are shown in Fig. 5. The profile distributions of the mean velocity predicted by the current model agree well with the experimental data, while the ske model predicts a much wider distribution. Significant improvement is also achieved in the prediction of the turbulent shear stress profile over the ske model in terms of both the centerline level and the overall distribution. The calculated spreading rates of these flows are compared with measurements and are shown in Table 3. The present model yields better predictions than the ske model; especially, the well-known spreading rate anomaly of planar and round jets (i.e., the measured spreading rate of a round jet is always smaller than that of a planar jet, but the model prediction usually contradicts the measurements) is removed completely.

4.3. Channel flow and boundary layer flows

Turbulent channel flow and boundary layer flows with/without pressure gradients were calculated to test the performance of the present model for wall bounded flows. Since the present model is proposed for turbulent flows away from the wall, the integration was carried out down to $y^+ = 80$, rather than to the wall, in the calculations. At $y^+ = 80$, DNS values were used as the boundary conditions for the turbulent channel flow and wall functions were used for the turbulent boundary layer flows.

The velocity profile for 2D fully developed turbulent channel flow at $Re_\tau = 395$ is shown in Fig. 6. This flow was calculated by Kim [19] using direct numerical simulation. Both the present model and the ske model agree reasonably well with the DNS data. Figure 7 shows the skin friction coefficient for the flat plate boundary layers with the Reynolds number up to $Re_\theta = 16{,}000$. Here, comparison is made with the experimental results of Wieghardt [20]. Both the present model and the ske model give good agreement with the experiments. Results for velocity profiles and boundary layer development can be found in Ref. [12]. Overall, the present model gives a slightly better prediction for boundary layer development.

Figure 8 shows the results for the Herring and Norbury flow [21], which is a boundary layer flow under favorable pressure gradient. The ske model gives better predictions for the skin friction

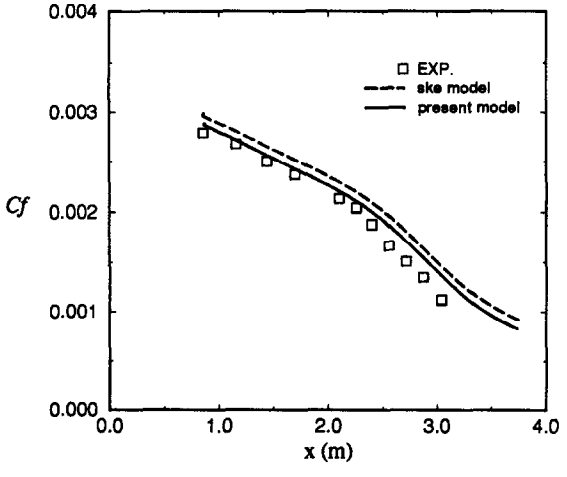

Fig. 10. Skin friction coefficient for the Samuel and Joubert [22].

Table 4. Comparison of the reattachment point locations

Case	Measurement	ske	Present
DS	6.1	4.99	6.02
KKJ	7 ± 0.5	6.35	7.50

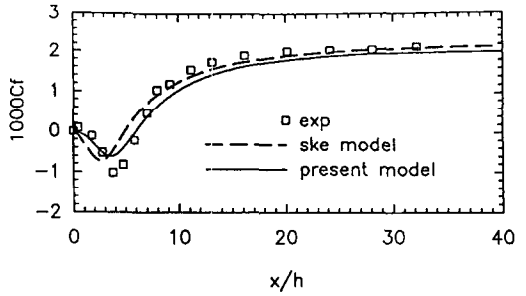

Fig. 11. Skin friction coefficient along the bottom wall. DS-case.

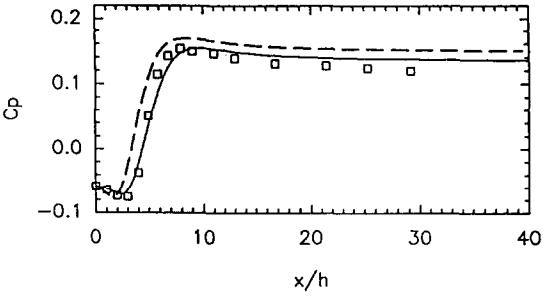

Fig. 12. Static pressure coefficient along the bottom wall. DS-case. Legend: see Fig. 11.

coefficient. However, the present model gives a better prediction for the boundary layer thickness (see Ref. [12] for detail.) The turbulent boundary layer under adverse pressure gradient studied by Bradshaw [22] and the turbulent boundary layer under increasingly adverse pressure gradient studied by Samuel and Joubert [23] were also calculated. The results are shown in Figs 9 and 10, respectively. In both cases, the present model gives better predictions.

4.4. Backward-facing step flows

The performance of the present model for complex recirculating flows is demonstrated through calculations for two backward-facing step flows, one (DS-case [24]) with smaller and the other (KKJ-case [25]) with larger step height, both of which have been extensively used to benchmark calculations of separated flows. The calculations were performed with a conservative finite-volume procedure. The convection terms of the governing equations were discretized by a second-order accurate and bounded differencing scheme [26], and all the other terms by the standard central differencing scheme. Sufficiently fine grids, with 201×109 points in the DS-case and 199×91 points in the KKJ-case, were used to establish numerical credibility of the solutions. The computational domain had a length of 50 step heights, one-fifth of which was placed upstream of the step. The experimental data were used to specify the inflow conditions, the fully-developed flow conditions were imposed at the outflow boundary, and the standard wall function approach [27] was used to bridge the viscous sublayer near the wall. Table 4 shows the comparison of the reattachment lengths. Figures 11–14 compare the skin friction, the pressure distribution along the bottom wall and the turbulent stress profiles in the DS-case. All the quantities were normalized by the step height h and the experimental reference free-stream velocity U_{ref}. The detailed comparison in both cases are given in Shih *et al.* [12]. The comparison shows that the overall performance of the present model is better than that of the ske model.

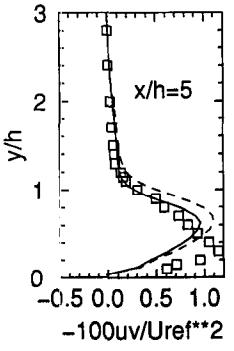

Fig. 13. Turbulent shear stress profiles. DS-case. Legend: see Fig. 11.

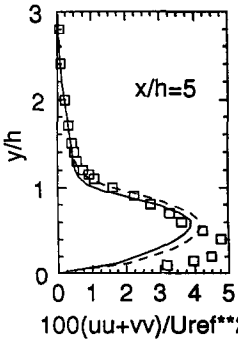

Fig. 14. Turbulent normal stress profiles. DS-case. Legend: see Fig. 11.

5. CONCLUDING REMARKS

A new k–ϵ eddy viscosity model is proposed in this paper. It consists of a new model dissipation rate equation and a new realizable eddy viscosity formulation. The new model dissipation rate equation is based on the dynamic equation for fluctuating vorticity. The new eddy viscosity formulation described in Section 3 ensures realizability and contains, as well, the effect of mean rotation on turbulence stresses. The present model is tested in various benchmark flows including: rotating homogeneous shear flows; boundary-free shear flows; channel and flat boundary layer flows with and without pressure gradients; and backward facing step flows. The results show that the present model performs better than the standard k–ϵ model in almost all the cases tested. The well-known spreading rate anomaly of planar and round jets is completely removed. In addition, the new model dissipation rate equation is expected to enhance the numerical stability in turbulent flow calculations, especially, when it is used in conjunction with more advanced closure schemes, such as second order closures. We have also just finished implementing the present model dissipation rate equation into the LRR [28] second order closure. Preliminary results show that the initial decay behavior of k and ϵ and the effect of rotation on both k and ϵ for initially isotropic rotating homogeneous shear flows are well captured.

REFERENCES

1. W. P. Jones and B. E. Launder, The calculations of low-Reynolds number phenomena with a two-equation model of turbulence. *Int. J. Heat Mass Transfer* **16,** 1119 (1973).
2. K. Y. Chien, Predictions of channel and boundary layer flow with a low-Reynolds-number turbulence model. *AIAA J.* **20,** 33 (1982).
3. Z. Yang and T.-H. Shih, A new time scale based k–ϵ model for near wall turbulence. *AIAA J.* **31,** 1191 (1993).
4. T.-H. Shih and J. L. Lumley, Kolmogorov behavior of near-wall turbulence and its application in turbulence modeling. NASA TM 105663.
5. J. Bardina, J. H. Ferziger and W. C. Reynolds, Improved turbulence models based on large eddy simulation of homogeneous, incompressible, turbulent flows. Rept. No. TF-19, Stanford University, Stanford, CA (1983).
6. J. L. Lumley, Some comments on turbulence. *Phys. Fluids* **4,** 203 (1992).
7. W. C. Reynolds, Fundamentals of turbulence for turbulence modeling and simulation. Lecture Notes for Von Karman Institute, Agard Report No. 755 (1987).
8. T.-H. Shih, J. Zhu and J. L. Lumley, A new Reynolds stress algebraic equation model. NASA TM, 106644 (1994).
9. H. Tennekes and J. L. Lumley, *A First Course in Turbulence.* MIT Press (1972).
10. M. S. Mohamed and J. C. Larue, The decay power law in grid-generated turbulence. *J. Fluid Mech.* **219,** 195 (1990).
11. S. Tavoularis and S. Corrsin, Experiments in nearly homogeneous turbulent shear flow with a uniform mean temperature gradient. *J. Fluid Mech.* **104,** 311 (1981).
12. T. H. Shih, W. W. Liou, A. Shabbir, Z. Yang and J. Zhu, A new k–ϵ eddy viscosity model for high Reynolds number turbulent flows—Model development and validation. NASA TM 106721 (1994).
13. R. P. Patel, An experimental study of a plane mixing layer. *AIAA J.* **29,** 67 (1973).
14. E. Gutmark and I. Wygnanski, The planner turbulent jet. *J. Fluid Mech.* **73,** 465 (1976).
15. L. J. S. Bradbury, The structure of the self-preserving jet. *J. Fluid Mech.* **23,** 31 (1965).
16. G. Hekestad, Hot-wire measurements in a plane turbulent jet. *J. Fluid Mech.* **32,** 721 (1965).
17. I. Wygnanski and H. E. Fiedler, The two dimensional mixing region. *J. Fluid Mech.* **41,** 327 (1970).
18. W. Rodi, A new method of analyzing hot-wire signals in highly turbulent flow and its evaluation in round jets. Disa Information, No. 17 (1975).
19. J. Kim, private communication.
20. K. Wieghardt, Equilibrium boundary layer at constant pressure. *Computation of Turbulent Boundary Layers* (Edited by D. E. Coles and E. A. Hirst), Vol. 2, pp. 98–123. AFSOR-IFP, Stanford Univ. (1968).
21. H. Herring and J. Norbury, Equilibrium boundary layer in mild negative pressure gradient. *Computation of Turbulent Boundary Layers* (Edited by D. E. Coles and E. A. Hirst), Vol. 2, pp. 249–258. AFSOR-IFP, Stanford Univ. (1968).
22. P. Bradshaw, Equilibrium boundary layer in moderate positive pressure gradient. *Computation of Turbulent Boundary Layers* (Edited by D. E. Coles and E. A. Hirst), Vol. 2, pp. 241–248. AFSOR-IFP, Stanford Univ. (1968).
23. A. E. Samuel and P. N. Joubert, A boundary layer developing in an increasingly adverse pressure gradient. *J. Fluid Mech.* **66,** 481 (1974).
24. D. M. Driver and H. L. Seegmiller, Features of a reattaching turbulent shear layer in divergent channel flow. *AIAA J.* **23,** 163 (1985).
25. J. Kim, S. J. Kline and J. P. Johnston, Investigations of separation and reattachment of a turbulent shear layer: flow over a backward-facing step, Rept. MD-37, Thermosciences Div., Dept of Mech. Eng., Stanford Univ. (1978).
26. J. Zhu, A low diffusive and oscillation-free convection scheme. *Comm. App. Num. Methods* **7,** 225 (1991).
27. B. E. Launder and D. B. Spalding, The numerical computation of turbulent flows. *Comput. Meths. App. Mech. Eng.* **3,** 269 (1974).
28. B. E. Launder, G. J. Reece and W. Rodi, Progress in the development of a Reynolds-stress turbulence closure. *J. Fluid Mech.* **68,** 537 (1974).